Multisolitons in a gauged Skyrme-Maxwell model

L. R. Livramento
BLTP, JINR, Dubna 141980, Moscow Region, Russia

Ya. Shnir
BLTP, JINR, Dubna 141980, Moscow Region, Russia
and Institute of Physics, Carl von Ossietzky University Oldenburg,
Germany Oldenburg D-26111, Germany

(Received 19 July 2023; accepted 29 August 2023; published 15 September 2023)

We construct new solutions of a $U(1)$ gauged Skyrme-Maxwell model of topological degrees $Q \leq 5$, which represent skyrmions coupled to magnetic fluxes. It is found that, generically, in the strong coupling limit, coupling to the magnetic field results in transformation of the configuration to the toroidally shaped skyrmions bounded to the local magnetic flux.

DOI: 10.1103/PhysRevD.108.065010

I. INTRODUCTION

The celebrated Skyrme model [1,2] serves as a prototype of a $(3+1)$-dimensional nonlinear field theory supporting topological solitons. This model possesses a wide variety of applications in several areas of physics (for a review, see [3–6]). It has been suggested [7,8] that the model may be of relevance for a low energy description of QCD, as the solitons are interpreted as nucleons and nuclei with the identification of the topological charge with the baryon number.

In its simplest form, the Skyrme model contains only three free parameters that set the length and energy scales and the mass of the scalar excitations, respectively. It successfully reproduces a number of qualitative features of nuclei in surprising accord with experiment [5,9]. However, the standard version of the Skyrme model is plagued with problems of prediction of binding energies for baryons and formation of cluster structures of nuclei.

Various modifications of the Skyrme model were considered over the last two decades to improve the situation. Among them are modifications of the potential [10–17], extended theories that incorporate scalar and vector mesons [18–25], and holographic models [26–28] inspired by the Atiyah-Manton construction of skyrmions [29,30]. It has been also suggested to include in the Lagrangian of the theory higher-order terms with additional couplings [31–37] or modify the Skyrme model to the form that supports self-duality equations [38–40].

The usual pion mass potential of the Skyrme model breaks the symmetry to the $SU(2)$ subgroup. This global symmetry can be gauged; inclusion of the Maxwell term leads to the $U(1)$ gauged Skyrme model that has been proposed in [41,42]. This approach is similar to the construction of the topological solitons in the $U(1)$ gauged $O(3)$ sigma model in $(2+1)$ dimensions [43–45], in the planar Skyrme-Maxwell model [46–48], and its modifications [49–53]. Static soliton solutions of the Faddeev-Skyrme-Maxwell theory in $3+1$ dimensions were discussed in [54,55]. In the context of the Skyrme model, such a modification was originally motivated by construction of a semiclassical model of interaction between a monopole and nucleons, the so-called Callan-Rubakov effect of the baryon decay catalysis [56,57]. Notably, extended Skyrme-Maxwell theory also can be derived in a holographic model via an expansion of a Yang-Mills field of calorons [58].

In [41,59] it was shown that coupling to the electromagnetic field significantly affects properties of the Skyrme field, even in the sector of topological degree 1. In particular, it violates the spherical symmetry of the configuration of topological degree 1 and induces a magnetic moment of the skyrmion. A gauged skyrmion possesses an electric charge and carries a magnetic flux. The existence of such solutions relies on the presence of the potential, and the electrostatic potential is restricted from above by the value of the pion mass [59]. However, electrically neutral solutions coupled to a magnetic flux exist in the limit of zero potential for arbitrary values of the gauge coupling.

The purpose of the current paper is to extend this analysis by analyzing how coupling to the magnetic flux affects the geometrical shape and energy of the static multisoliton solutions of the $U(1)$ gauged Skyrme model of topological degrees $Q = 1$–5.

This paper is organized as follows. In Sec. II, we introduce the model and define the topological charge of the gauged skyrmions. In Sec. III, we define the parametrization of the fields to be used in finding the numerical solutions and introduce reduced axially symmetric *Ansätze*. In Sec. IV, we present our full 3D numerical scheme and discuss the numerical results. Finally, in Sec. V, we present our conclusions and further remarks.

II. THE MODEL

The Lagrangian density of the $(3+1)$-dimensional, $U(1)$ gauged massive Skyrme-Maxwell model is defined as [41,42,59,60]

$$\begin{aligned}\mathcal{L} = &-\frac{1}{4}\mathcal{F}_{\mu\nu}\mathcal{F}^{\mu\nu} + \frac{f_\pi^2}{2}\mathcal{D}_\mu\phi^a\mathcal{D}^\mu\phi^a \\ &-\frac{1}{4a_0^2}[(\mathcal{D}_\mu\phi^a\mathcal{D}^\mu\phi^a)^2 - (\mathcal{D}_\mu\phi^a\mathcal{D}_\nu\phi^a)(\mathcal{D}^\mu\phi^b\mathcal{D}^\nu\phi^b)] \\ &- m_\pi^2(1-\phi_0). \end{aligned} \tag{1}$$

Here we employ the $O(4)$ sigma model representation of the Skyrme field as an S^3-valued field $\phi^a = (\phi_0, \phi_k)$ subject to the constraint $\phi^a \cdot \phi^a = 1$. In the context of application of the Skyrme model to nuclear physics, the component ϕ_0 has the interpretation as a scalar meson, while the isotriplet ϕ_k, $k = 1, 2, 3$ corresponds to the pions. Note that the inclusion of the potential term is necessary to stabilize the model both with respect to isorotations [61,62] and coupling to the electromagnetic field [59].

The electromagnetic field strength tensor is $\mathcal{F}_{\mu\nu} = \partial_\mu\mathcal{A}_\nu - \partial_\nu\mathcal{A}_\mu$, $a = 0, \ldots, 3$ and the covariant derivative of scalar field ϕ^a is defined in terms of the four-potential $\mathcal{A}_\mu$ as [41,42]

$$\begin{aligned}&\mathcal{D}_\mu\phi_\alpha = \partial_\mu\phi_\alpha - e\mathcal{A}_\mu\varepsilon_{\alpha\beta}\phi_\beta, \qquad \mathcal{D}_\mu\phi_A = \partial_\mu\phi_A, \\ &\alpha,\beta = 1,2, \qquad A = 0,3. \end{aligned} \tag{2}$$

The physical vacuum corresponds to $\mathcal{D}_\mu\phi_\alpha = 0$, $\mathcal{F}_{\mu\nu} = 0$ and $\phi_0 = 1, \phi_k = 0$.

In natural units the Skyrme constant a_0 is dimensionless, while the pion decay constant f_π and the pion mass parameter m_π are of dimension of mass. Two of these parameters may be scaled away by introducing the energy and length scales $f_\pi/(4a_0)$ and $2/(a_0 f_\pi)$, respectively. The rescaled pion mass parameter is $m = 2m_\pi/(a_0 f_\pi)$ and the gauge coupling becomes $g \equiv e/a_0$. Then the rescaled Lagrangian of the Skyrme-Maxwell model can be written as

$$\begin{aligned}\mathcal{L} = &-\frac{1}{2}F_{\mu\nu}F^{\mu\nu} + D_\mu\phi^a D^\mu\phi^a - \frac{1}{2}(D_\mu\phi^a D^\mu\phi^a)^2 \\ &+\frac{1}{2}(D_\mu\phi^a D_\nu\phi^a)(D^\mu\phi^b D^\nu\phi^b) \\ &- 2m^2(1-\phi_0), \end{aligned} \tag{3}$$

where

$$\begin{aligned}&D_\mu\phi_\alpha = \partial_\mu\phi_\alpha - gA_\mu\varepsilon_{\alpha\beta}\phi_\beta, \qquad D_\mu\phi_A = \partial_\mu\phi_A, \\ &\alpha,\beta = 1,2, \qquad A = 0,3. \end{aligned} \tag{4}$$

The Skyrme-Maxwell model (3) is invariant with respect to the local $U(1)$ gauge transformations

$$\phi_1 + i\phi_2 \to e^{-ig\alpha}(\phi_1 + i\phi_2), \qquad A_\mu \to A_\mu + \partial_\mu\alpha, \tag{5}$$

where α is any real function of coordinates. We will fix the gauge setting $A_0(\infty) = 0$.

The model (3) has a conserved, integer-valued topological charge, the degree of the map $S^3 \mapsto S^3$, which can be written as

$$\begin{aligned}Q_T &= \int d^3x q(\vec{r}) \\ &= -\frac{1}{12\pi^2}\int d^3x \varepsilon_{abcd}\varepsilon_{ijk}\phi^a\partial_i\phi^b\partial_j\phi^c\partial_k\phi^d. \end{aligned} \tag{6}$$

However, such a quantity is not invariant with respect the $U(1)$ gauge transformations (5). Let us introduce the quantity

$$Q_g = -\frac{1}{24\pi^2}\int d^3x \varepsilon_{ijk}\mathrm{Tr}(D_i U U^{-1} D_j U U^{-1} D_k U U^{-1}), \tag{7}$$

where $U = \phi_0\mathbb{1} + i\phi_i\tau_i$ is the Skyrme field, $D_i U = \partial_i U - igA_i[Q_c, U]$, $Q_c = \mathrm{diag}(\frac{2}{3}, -\frac{1}{3})$ is the charge matrix, and τ_i are the Pauli matrices. The quantity (7) can be obtained from the usual topological charge via replacing the partial derivatives by the covariant derivatives [41,59]. The $U(1)$ gauge covariant generalization of the usual topological charge (6) associated with Skyrme-Maxwell theory (3) and the gauge transformation (5) is defined by subtracting the magnetic contribution $Q_{\mathrm{mag}} = \int d^3x \frac{ig}{32\pi^2}(\varepsilon_{ijk}F_{jk})\mathrm{Tr}(\{\tau_3, \partial_i U\}U^{-1})$ from (7), i.e.,

$$Q \equiv Q_g - Q_{\mathrm{mag}} = \int d^3x q + \int d^3x \partial_i\Lambda_i, \tag{8}$$

where the surface term depends on the boundary conditions imposed on the fields [41,58],

$$\Lambda_i = -\frac{g}{4\pi^2}\varepsilon_{ijk}A_j(\phi_3\partial_k\phi_0 - \phi_0\partial_k\phi_3). \tag{9}$$

In the Abelian Skyrme-Maxwell model (3), the flux of Λ_i is vanishing, thus $Q = Q_T$ [41,59].

The stress-energy tensor that follows from (1) is

$$T^{\mu\nu} = T^{\mu\nu}_{(M)} + T^{\mu\nu}_{(S)}, \tag{10}$$

where the electromagnetic contribution is

$$T^{\mu\nu}_{(M)} = -2F^{\mu\sigma}F^{\nu}{}_{\sigma} + \frac{\eta^{\mu\nu}}{2}F_{\alpha\beta}F^{\alpha\beta}, \tag{11}$$

and the stress-energy tensor of the $U(1)$ gauged skyrmions is

$$T^{\mu\nu}_{(S)} = 2[D^{\mu}\phi_a D^{\nu}\phi^a - (D^{[\mu}\phi^a D^{\alpha]}\phi^b)(D^{[\nu}\phi_a D_{\alpha]}\phi_b)] - \eta^{\mu\nu}\left((D_\alpha\phi_a)^2 - \frac{1}{2}(D_{[\alpha}\phi_a D_{\beta]}\phi_b)^2 - 2m^2(1-\phi_0)\right). \tag{12}$$

For stationary solutions in the static gauge, the Lagrangian and Hamiltonian of the Skyrme-Maxwell model can be written, respectively, as

$$\mathcal{L}_{\text{static}} = -\mathcal{H}_1 + \mathcal{H}_2, \qquad \mathcal{H}_{\text{static}} = \mathcal{H}_1 + \mathcal{H}_2, \tag{13}$$

where $\mathcal{H}_1$ and $\mathcal{H}_2$ are non-negative terms given by

$$\begin{aligned}
\mathcal{H}_1 &= \frac{1}{2}|F_{ij}|^2 + |D_i\phi_a|^2 + \frac{1}{2}|D_{[i}\phi_a D_{j]}\phi_b|^2 + 2m^2(1-\phi_0),\\
\mathcal{H}_2 &= |\partial_i A_0|^2 + g^2 A_0^2 M_\phi^2, \quad \text{with}\\
M_\phi^2 &\equiv \left[(1+|\partial_i\phi_A|^2)|\phi_\alpha|^2 + \frac{1}{4}|\partial_i(|\phi_A|^2)|^2\right],
\end{aligned} \tag{14}$$

where $|\partial_i A_0|^2 = \partial_i A_0 \partial_i A_0$, and so on. Clearly, the term $\mathcal{H}_2$ yields the Gauss law. Imposing the Coulomb gauge $\partial_i A_i = 0$, we can write the static Maxwell equations of the system

$$\begin{aligned}
\partial_j^2 A_0 &= g^2 M_\phi^2 A_0,\\
\partial_j^2 A_i &= -g\varepsilon_{\alpha\beta}\phi_\beta[(1 + D_j\phi_a D_j\phi_a)D_i\phi_\alpha\\
&\quad - (D_j\phi_a D_j\phi_\alpha)D_i\phi_a].
\end{aligned} \tag{15}$$

III. $U(1)$ GAUGED SKYRMIONS

Hereafter, we consider the case of vanishing electrostatic potential $A_0(\vec{r}) = 0$, so the Gauss law is satisfied trivially. Consequently, the electric charge vanishes and $\mathcal{H}_2 = 0$. The total static energy of the gauged skyrmions can be written as

$$E = E_2 + E_4 + E_0 + E_{\text{em}}, \tag{16}$$

where

$$\begin{aligned}
E_2 &= \frac{1}{12\pi^2}\int d^3x |D_i\phi_a|^2,\\
E_4 &= \frac{1}{12\pi^2}\int d^3x \frac{1}{2}|D_{[i}\phi_a D_{j]}\phi_a|^2,\\
E_0 &= \frac{1}{12\pi^2}\int d^3x 2m^2(1-\phi_0),\\
E_{\text{em}} &= \frac{1}{12\pi^2}\int d^3x \frac{1}{2}|F_{ij}|^2,
\end{aligned} \tag{17}$$

and we make use of the standard normalization of the energy functional by the factor $12\pi^2$.

The critical points of the total energy functional (16) should satisfy the arguments of Derrick's theorem [63]. Under a scale transformation $x_i \to x_i' = \lambda x_i$, the scalar fields ϕ_a and the four-potential transform as $\phi_a \to \phi_a$ and $A_\mu \to A_\mu'(\vec{x}') = \lambda^{-1}A_\mu(\vec{x})$. Thus,

$$E(\lambda) = \lambda^{-1}E_2 + \lambda(E_4 + E_{\text{em}}) + \lambda^{-3}E_0, \tag{18}$$

and

$$\partial_\lambda^2 E(\lambda = 1) = 2[E_2 + 6E_0] \geq 0.$$

The corresponding virial identity follows from the condition $\partial_\lambda E(\lambda = 1) = 0$, it gives $E_2 + 3E_0 = E_4 + E_{\text{em}}$, which can also can be obtained from (12) using the von Laue stability condition $\int d^3x T_i^i = 0$ [64,65].

There is a variety of classical multisoliton solutions of the usual Skyrme model constructed numerically over last three decades, see [3,4]. As the electromagnetic interaction is decoupled, the basic unit charge skyrmion represents a spherically symmetric hedgehog [1,2]. Skyrmions of higher topological degrees may possess much more complicated symmetries; the shape of the multisoliton configuration strongly depends on the particular choice of the potential and corresponding character of asymptotic decay of the fields. Coupling to the electromagnetic field yields an additional interaction: our full 3D numerical simulations confirmed that $U(1)$ gauged skyrmions of topological degrees $Q = 1, 2$ are axially symmetric [41,59]. These skyrmions can be constructed using a general reduced *Ansatz* [42,61,66,67],

$$\phi_1 + i\phi_2 = \psi_1(r,\theta)e^{in\varphi}, \quad \phi_3 = \psi_2(r,\theta), \quad \phi_0 = \psi_3(r,\theta), \tag{19}$$

where n is an integer that counts the winding of the unit vector field $\vec{\psi} = (\psi_1, \psi_2, \psi_3)$, $|\psi|^2 = 1$ in the equatorial plane. In a more general case, the topological charge of the axially symmetric skyrmions is given by the product of two integers, $Q = mn$, where n is the phase winding number (19) and m is a number of twists along the toroidal fundamental cycle of the torus; see, e.g., [68,69]. For all solutions we are discussing here, the number of twists $m = 1$, so $Q = n$ [42,61,66]. Note that the *Ansatz* (19) also can be used to construct saddle point solutions of the Skyrme model, which

represent chains of interpolating skyrmion-antiskyrmions of topological degree $\pm n$ [66,68].

Since in the present study we do not consider electrically charged skyrmions, the gauge field is parametrized by the magnetic potential solely,

$$A \equiv A_\mu dx^\mu = A_\varphi(r,\theta)d\varphi. \tag{20}$$

All four functions that parametrize the axially symmetric *Ansätze* (19) and (20) depend on the radial variable r and the polar angle θ. Within this *Ansatz*, the Skyrme-Maxwell static Lagrangian (13), normalized by the factor $12\pi^2$, and the energy (16) become

$$L = -\frac{1}{6\pi}\int d\theta dr r^2 \sin\theta[\mathcal{F} + \mathcal{L}_2 + \mathcal{L}_4 + 2m^2(1-\psi_3)],$$
$$E = -L, \tag{21}$$

where

$$\mathcal{F} \equiv \frac{1}{r^2\sin^2\theta}\left(A_{\varphi,r}^2 + \frac{A_{\varphi,\theta}^2}{r^2}\right),$$
$$\mathcal{L}_2 \equiv \psi_{a,r}^2 + \frac{\psi_{a,\theta}^2}{r^2} + \psi_1^2\frac{(n+gA_\varphi)^2}{r^2\sin^2\theta}, \tag{22}$$

$$\mathcal{L}_4 \equiv \frac{1}{r^2}[(\psi_{3,\theta}\psi_{2,r} - \psi_{2,\theta}\psi_{3,r})^2 + (\psi_{2,\theta}\psi_{1,r} - \psi_{1,\theta}\psi_{2,r})^2 + (\psi_{3,\theta}\psi_{1,r} - \psi_{1,\theta}\psi_{3,r})^2] + \psi_1^2\frac{(n+gA_\varphi)^2}{r^2\sin^2\theta}\left(\psi_{a,r}^2 + \frac{\psi_{a,\theta}^2}{r^2}\right). \tag{23}$$

Here a comma denotes partial differentiation, i.e., $A_{\varphi,r} \equiv \frac{\partial A_\varphi}{\partial r}$, etc. The corresponding static field equations can be obtained from the variation of the effective Lagrangian (21) with respect to the functions parametrizing the *Ansätze* (19) and (20).

It was pointed out [66] that the solutions of the Skyrme model constructed via the reduced *Ansatz* (19) have certain similarity with hopfions in the Faddeev-Skyrme model [70–72]. Furthermore, in the $U(1)$ gauged Skyrme model, time-dependent gauge transformations (5) are associated with isorotations of the scalar field [42]. Hence, one of the components of the pion triplet can be set to zero, effectively truncating the model to the $U(1)$ gauged Faddeev-Skyrme-Maxwell theory [54,55]. However, there still is topological difference between such configurations and axially symmetric hopfions classified by $\pi_3(S^2)$. Below, we will see that numerical simulations clearly confirm the distinct distribution of the fields of the axially symmetric hopfions and the $U(1)$ gauged skyrmions.

IV. NUMERICAL SCHEME

To find stationary points of the energy functional (16), we use a suitable combination of the gradient descendent method, implemented for solving the system of Euler-Lagrange equations for the scalar field, and the Newton-Raphson method for solving the Maxwell equation for the magnetic potential. Generally, we do not impose any restrictions of symmetry; however, in order to check the consistency of our numerical calculations, in case of the axially symmetric solitons with topological charges $Q = 1, 2$, we compare the results of full 3D simulations with reduced solutions of the truncated system (21).

Most of our simulations are performed on cubic grids of $(121)^3$ points with a lattice spacing $\Delta x = 0.1$ and adaptive step size. We impose Dirichlet boundary conditions $\phi^a = (1,0,0,0)$ on the boundary of the cube and make use of a fourth-order finite difference scheme. The boundary conditions on the magnetic potential are $A_\phi(0) = A_\phi(\infty) = 0$. To avoid local minima of the energy functional (16) for all charges from 1 to 5, we accept only results that provide the same global minimizer of E for different initial guesses generated by the rational map approximation, the product *Ansatz*, and the axially symmetric *Ansätze* (19) and (20).[1] We also check the results of our fully three-dimensional numerical simulations with those obtained by solving the reduced two-dimensional system of equations for axially symmetric solutions of degrees 1 and 2. In the latter case, we put the system on a square domain with 70^2 points and map the infinite interval of the variable r onto the compact radial coordinate $x = \frac{r}{2+r} \in [0:1]$.

The gradient flows of the scalar field EL_{ϕ_a} and the gauge field EL_{A_a} are

$$EL_{\phi_a} \equiv \frac{1}{2}\left(\frac{\delta L_{\text{static}}}{\delta\phi_a} - \phi_a\sum_{b=0}^{3}\phi_b\frac{\delta L_{\text{static}}}{\delta\phi_b}\right), \tag{24}$$

$$EL_{A_i} \equiv \partial_j^2 A_i + g\varepsilon_{\alpha\beta}\phi_\beta[(1 + D_j\phi_a D_j\phi_a)D_i\phi_\alpha - (D_j\phi_a D_j\phi_\alpha)D_i\phi_a], \qquad EL_{A_0} \equiv 0, \tag{25}$$

respectively. Energy minima of the system correspond to $EL_{\phi_a} = 0, EL_{A_i} = 0$; the accuracy check of our simulations is to evaluate the root-mean-square deviation of the Euler-Lagrange gradients

$$\Delta_E = \sqrt{\frac{1}{N}\sum_{a=0}^{4}(|EL_{\phi_a}|^2 + |EL_{A_a}|^2)}, \tag{26}$$

[1]The rational map is a powerful *Ansatz* to constructing a very symmetric initial field configuration that leads to the global energy minimizer for the Skyrme model. However, in our simulations, for $Q = 4$ and $g > 0$, these initial settings did not lead to the global minimizer, which can be obtained by starting with four $Q = 1$ skyrmions or two $Q = 2$ skyrmions combined through the product *Ansatz*.

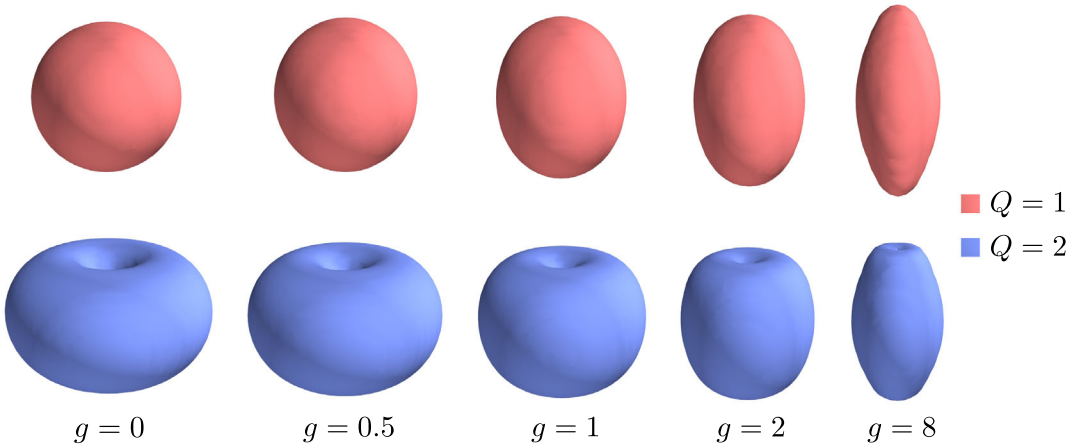

FIG. 1. Isosurfaces of the total energy density distributions of the gauged skyrmions with $Q = 1$ (top row) and $Q = 2$ (bottom row) are displayed for some values of g for $\mathcal{E} = 0.08$. In each row, all of the solutions are plotted at the same scale.

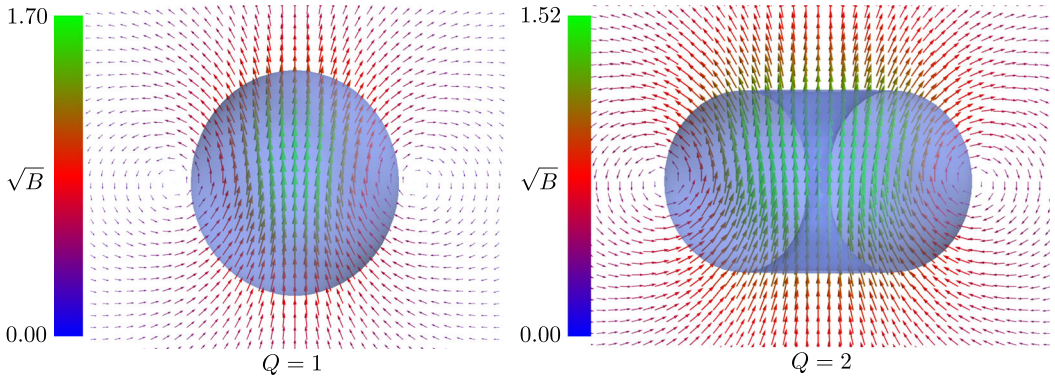

FIG. 2. Distribution of the magnetic field $\vec{B}$ in the x–z plane is displayed for the axially symmetric gauged skyrmions of topological degrees 1 (left) and 2 (right) for $g = 0.5$. The length of the plotted vectors is proportional to the magnitude of $\vec{B}/\sqrt{B}$, where $B \equiv |\vec{B}|$. The translucent blue surface is a level set of constant total energy density for $\mathcal{E} = 0.1$.

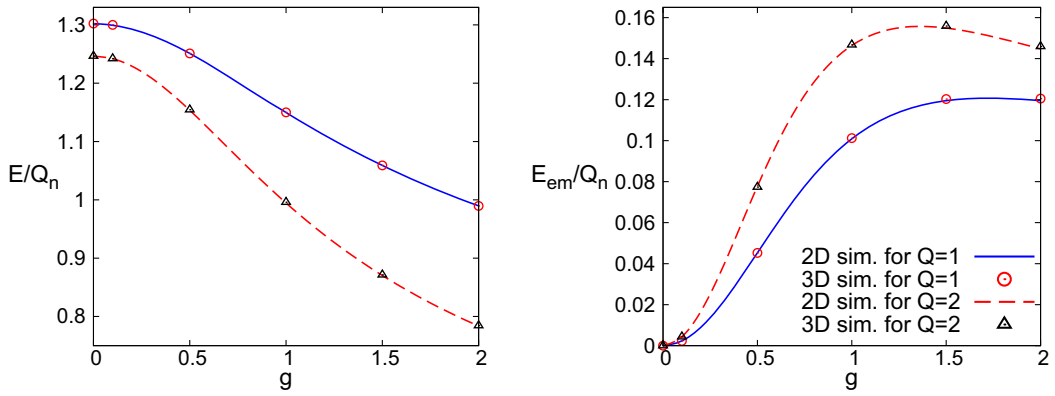

FIG. 3. The total energy E and the electromagnetic energy E_{em} of the axially symmetric skyrmions with $Q = 1, 2$, per unit charge. The curves and the dots correspond to the results obtained using reduced axially symmetric *Ansätze* (19) and (20) and with fully three-dimensional numerical simulations, respectively.

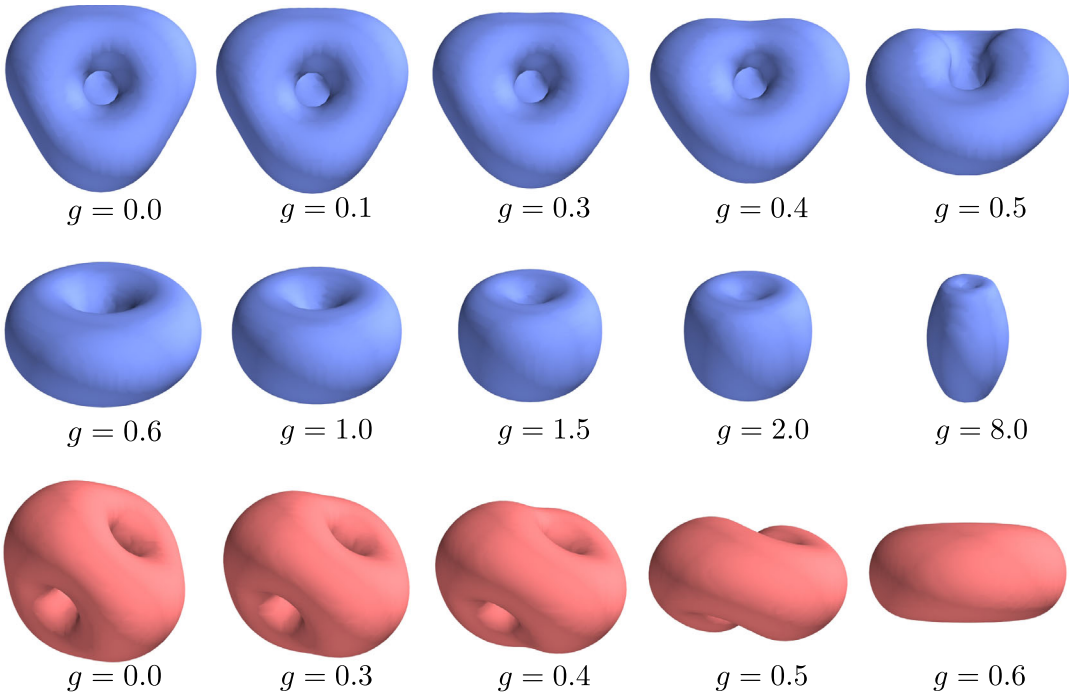

FIG. 4. Isosurfaces of the total energy density of the gauged skyrmion of degree $Q = 3$ for some set of values of g at $\mathcal{E} = 0.08$. The bottom row displays the side view of these skyrmions. In each row, all of the solutions are plotted at the same scale.

where N is the number of points of the lattice. Typically, for our numerically determined minima on a cubic lattice, we obtain $\Delta_E \sim 10^{-8}$.[2] As a further check of our numerics, we calculate numerically the topological charge Q_n through (6) and compare it to its true integer value Q, $|1 - Q_n/Q| \sim 3 \times 10^{-4}$. We also checked that the virial relation is satisfied within 1%–2% accuracy. In the case of the 2D simulations, the errors are reduced further by an order of magnitude.

V. NUMERICAL RESULTS

First, we considered axially symmetric gauged skyrmions with topological charges $Q = 1$, 2. As the gauge coupling gradually increases from $g = 0$, the energy of the configuration decreases[3] since the local magnetic flux is formed in the equatorial plane and core of the soliton shrinks; see Figs. 1 and 2. The position of the circular flux is associated with a minimum of the magnetic potential A_φ. The electromagnetic energy is initially increasing, however, its contribution starts to decrease as g becomes larger than $g \sim 1$, see Fig. 3. The total magnetic flux of the configuration is zero, and it is coupled to the skyrmion providing its magnetic moment.

As the coupling becomes stronger, the magnetic potential develops a plateau in the equatorial plane, where $gA_\varphi + n \sim 0$. Here the integer n is to the winding number of the unit vector field $\vec{\psi}$ (19). This corresponds to a string of magnetic flux through the center of the configuration. The flux is nontopologically quantized in units of 2π and carries n quanta. It is known that such a situation is common for all $U(1)$ gauged solitons, like hopfions in

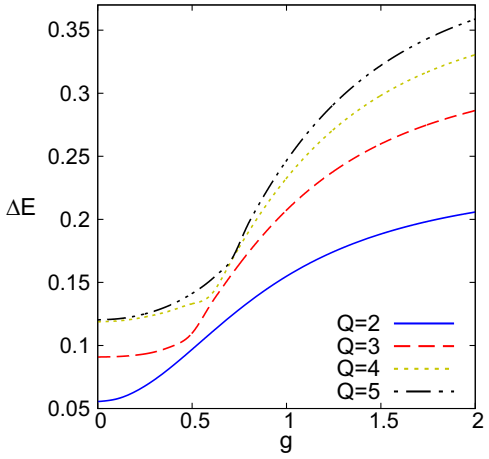

FIG. 5. The binding energy per topological charge unit $\Delta E(g) \equiv E_{Q=1}(g) - E_Q(g)/Q$ of the skyrmions with $Q = 2$–5. The values of the energies are shown in the lines plotted in Figs. 3 and 9.

[2]The accuracy for nontoroidal $Q = 4$ gauged skyrmions ($g = 0.1, \ldots, 0.6$) decreases to $\Delta_E < 6 \times 10^{-5}$. In addition, in such a case the maximum values of the modulus of the gradients (24) over all the lattice points satisfies max $|EL_a| < 8 \times 10^{-4}$ and max $|EL_{A_a}| < 10^{-7}$.

[3]However, the binding energy of the gauged skyrmions per unit charge increases [41].

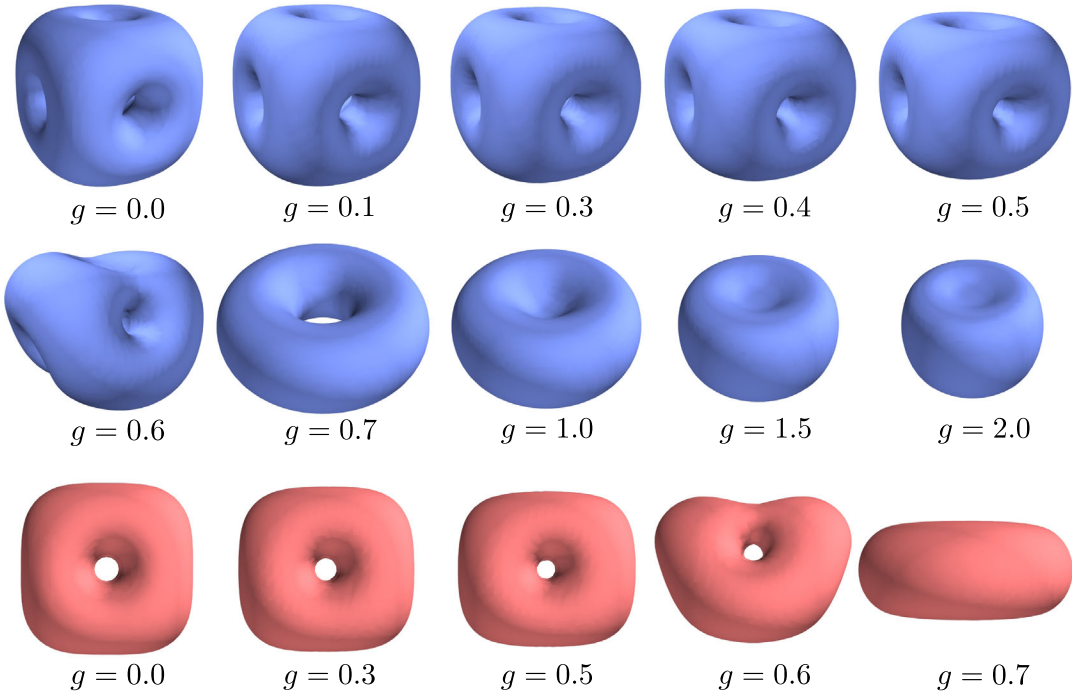

FIG. 6. Isosurfaces of the total energy density of the gauged skyrmion of degree $Q = 4$ for some set of values of g at $\mathcal{E} = 0.08$. The bottom row displays the side view of these skyrmions. In each row, all of the solutions are plotted at the same scale.

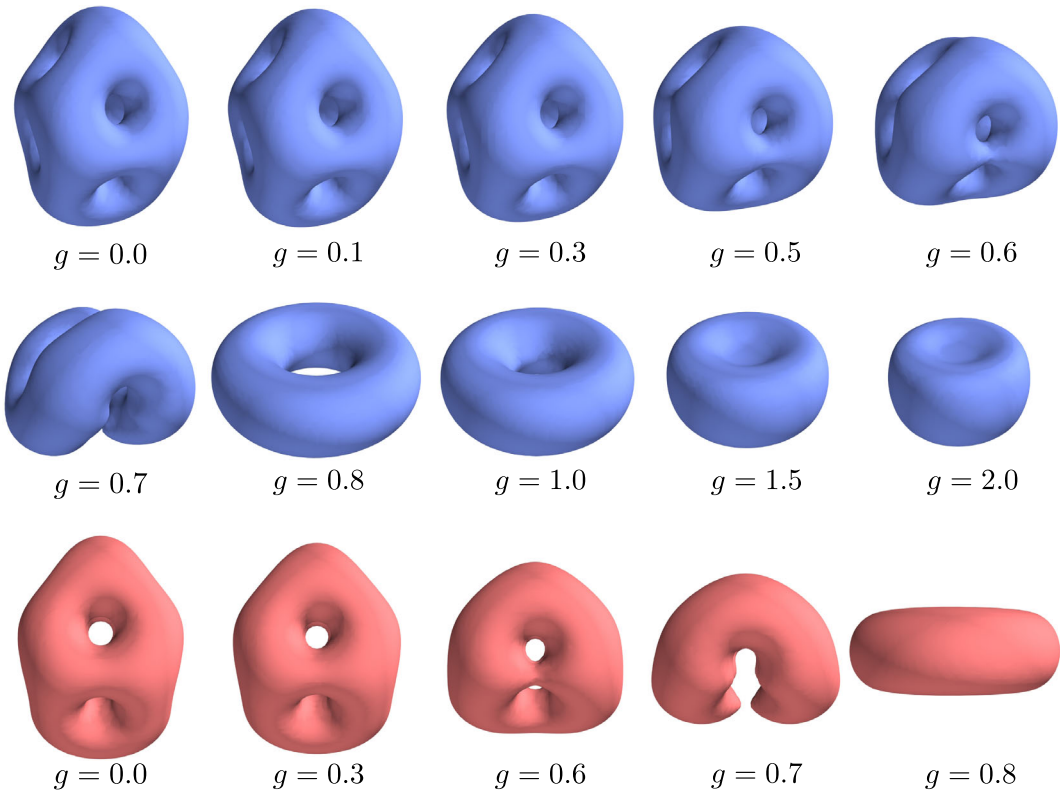

FIG. 7. Isosurfaces of the total energy density of the gauged skyrmion of degree $Q = 5$ for some set of values of g at $\mathcal{E} = 0.08$. The bottom row displays the side view of these skyrmions. In each row, all of the solutions are plotted at the same scale.

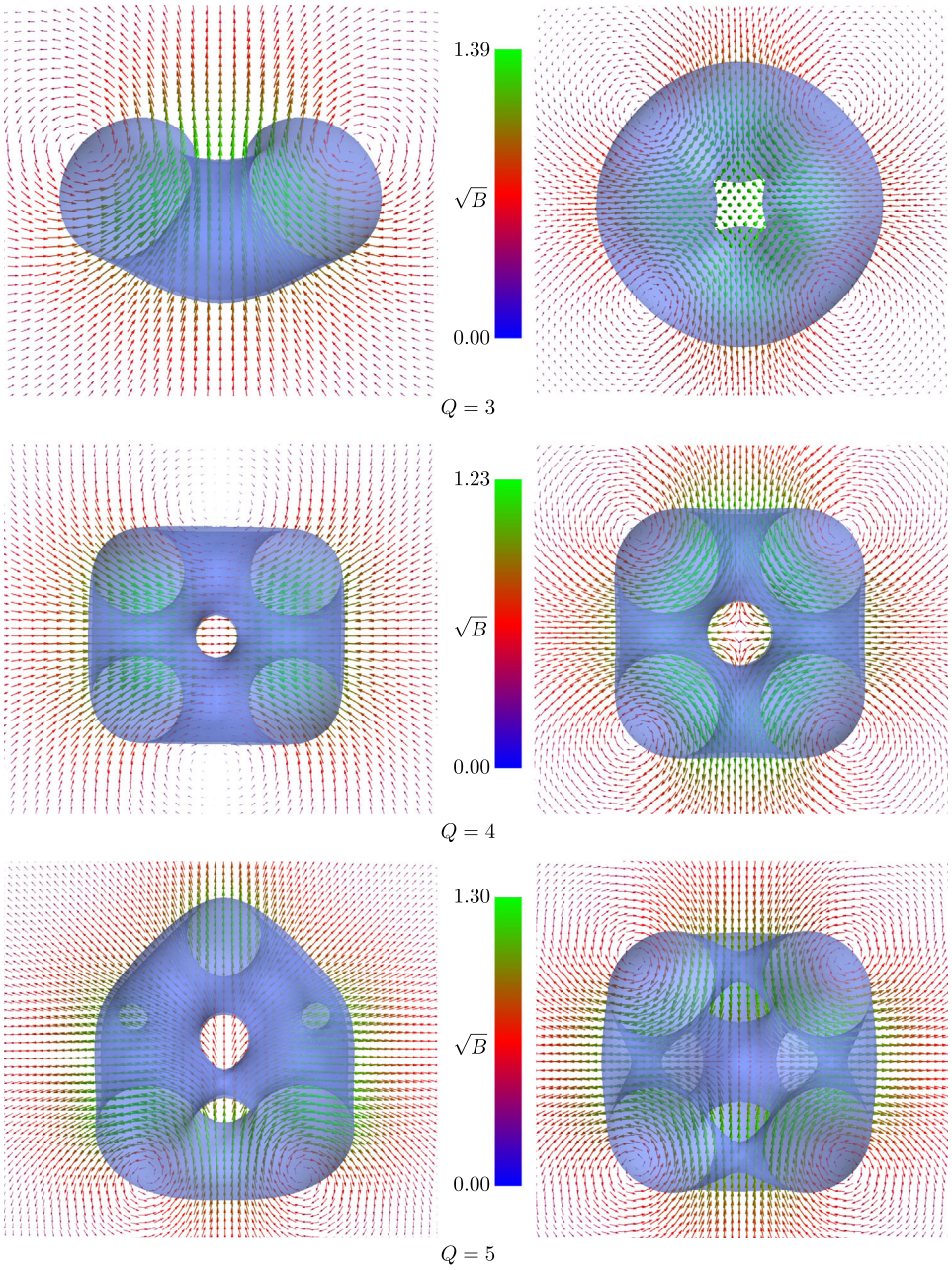

FIG. 8. Distributions of the magnetic field $\vec{B}$ in the x–z plane (left) and in the x–y plane (right) for the gauged skyrmions of topological degrees 3–5 for $g = 0.5$. The length of the plotted vectors is proportional to the magnitude of $\vec{B}/\sqrt{B}$, where $B \equiv |\vec{B}|$. The translucent blue surface is a level set of constant total energy density for $\mathcal{E} = 0.1$.

the Faddeev-Skyrme-Maxwell model [54], gauged planar skyrmions [46–48], and gauged $O(3)$ lumps [43].

Turning now to solitons of higher degrees, we consider gauged skyrmions with $Q = 3$–5. In the ungauged limit, the $Q = 3$ skyrmion has tetrahedral symmetry; coupling to the magnetic flux breaks it down. Figure 4 displays the corresponding isosurfaces of the total energy densities for the gauged skyrmions for some set of values of the gauge coupling g up to $g = 8$. Clearly, the geometrical shape of the $Q = 3$ soliton varies from a regular tetrahedron at $g = 0$ to a torus at $g \leq 0.6$. Note that at $g \approx 0.5$ the energy density distribution of a gauged skyrmion takes the shape of a bent torus, which is exactly the shape of the ground state hopfion with topological charge 3. As said above, there is an evident similarity between the axially symmetric solution of the Skyrme-Maxwell theory and hopfions; the curve of positions of minima of the component ϕ_0 correspond to the position curve of the hopfion. Interestingly, this similarity also persists for the charge 3 gauged solitons, which do not possess axial symmetry.

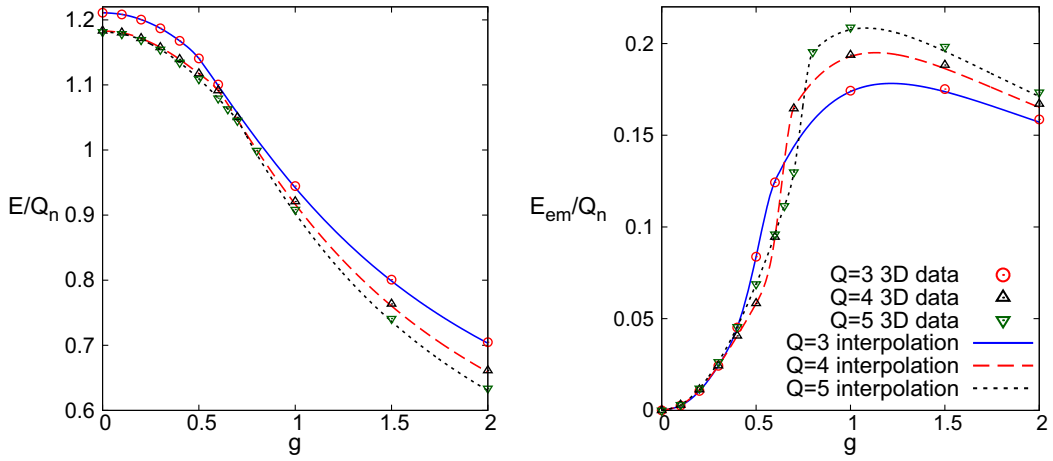

FIG. 9. The total energy E and the electromagnetic energy $E_{\rm em}$ of the skyrmions with $Q = 3$–5, per unit charge. The dots correspond to the values obtained through fully three-dimensional numerical simulations; the curves are plotted using cubic interpolation and the data of the fully three-dimensional simulations for $g \leq 0.5$, 0.6, 0.7 for, respectively, $Q = 3$, 4, 5, and the results obtained inside the axially symmetric *Ansatz* for $g \geq 0.6$, 0.7, 0.8, respectively.

Considering the binding energy of the gauged skyrmions, we confirm confirm earlier results that the binding energy of the gauged skyrmions per unit charge increases [41]. Figure 5 displays the binding energy of the $Q = 2$–5 gauged skyrmions vs gauge coupling g. Evidently, it moves further from the topological bound as Q increases.

Physically, the transformation of a skyrmion from a configuration with discrete symmetry to the toroidal state corresponds to a phase transition induced by the axially symmetric magnetic field. This effect is similar to transitions to toroidal skyrmions in the Skyrme model with symmetry breaking potential [69].

The distribution of the magnetic field of the $Q = 3$ configuration is different from the case of axially symmetric skyrmions, see Fig. 8. In the decoupled limit $g = 0$, the total energy density distribution is tetrahedrally symmetric, and appearance of the magnetic flux that encircles the skyrmion breaks this symmetry. The total magnetic flux is zero, and the four lumps at the vertices of the tetrahedron are bounded to local magnetic fluxes, as displayed in Fig. 8. As the gauge coupling increases, these local fluxes move toward the center of the configuration, and they merge into a single return flux penetrating the center of the gauged $Q = 3$ skyrmion as $g \geq 0.6$.

Numerical simulations show that qualitatively the same pattern appears for the gauged skyrmions of higher degrees, see Figs. 6, 7, and 9. The usual $Q = 4$ skyrmion for $g = 0$ is octahedrally symmetric; the ungauged $Q = 5$ configuration can be approximately described by a bounded system of $4 + 1$ skyrmions.

As the gauge coupling increases, the contribution of the electromagnetic energy is increasing at first, and it is maximal as $g \sim 1$; see Fig. 9. This effect is related to deformations of the skyrmions and formation of magnetic flux.

The structure of the magnetic field follows the pattern above: in the weak coupling regime, there is a circular magnetic flux tube, which encircles the skyrmions of degrees 3–5. This flux is linked to the four return local fluxes, as seen in the right column of Fig. 8, where the circular magnetic field crosses the isosurface of total energy density of $\mathcal{E} = 0.1$. Further increase of the gauge coupling drives the skyrmions toward an axially symmetric solution bounded with a toroidal magnetic field with a flux along the symmetry z axis of the configuration, and the circular magnetic flux orthogonal to the x–z plane, analogously to what can be seen for $Q = 2$ on the right plot in Fig. 2. The transformation to the toroidal $Q = 4$ and $Q = 5$ skyrmions takes place around $g = 0.7$ and $g = 0.8$, respectively. Clearly, the behavior of the magnetic field is more complex for non-axially-symmetric gauge skyrmions, and its magnitude tends to be stronger inside the core of the skyrmion. Figure 8 displays the magnitude and direction of the magnetic field for $g = 0.5$.

In Fig. 10 we illustrate transition to toroidal gauged skyrmions. Here, we visualize the field configurations by plotting isosurfaces of the field components $\phi_0 = -0.9$, $\phi_3 = \pm 0.9$, and $|\Phi| = 0.9$, where $\Phi \equiv \phi_1 + i\phi_2$, for some set of values of the gauge coupling g. The coloring scheme displays the phase of the component Φ. This also allows us to compare the toroidal skyrmions with hopfions, the tubelike isosurface $\phi_0 = -0.9$ can be set into correspondence with the position curve of the soliton, and it is defined as the set of points where the field ϕ_0 is as far as possible from the boundary vacuum value $\phi_0 = 1$.

Recall that the topological charge of the toroidal skyrmions (6) is given by the product of two integers, $Q = mn$, were n is the phase winding number and m is a number of twists along the fundamental cycle of the torus.

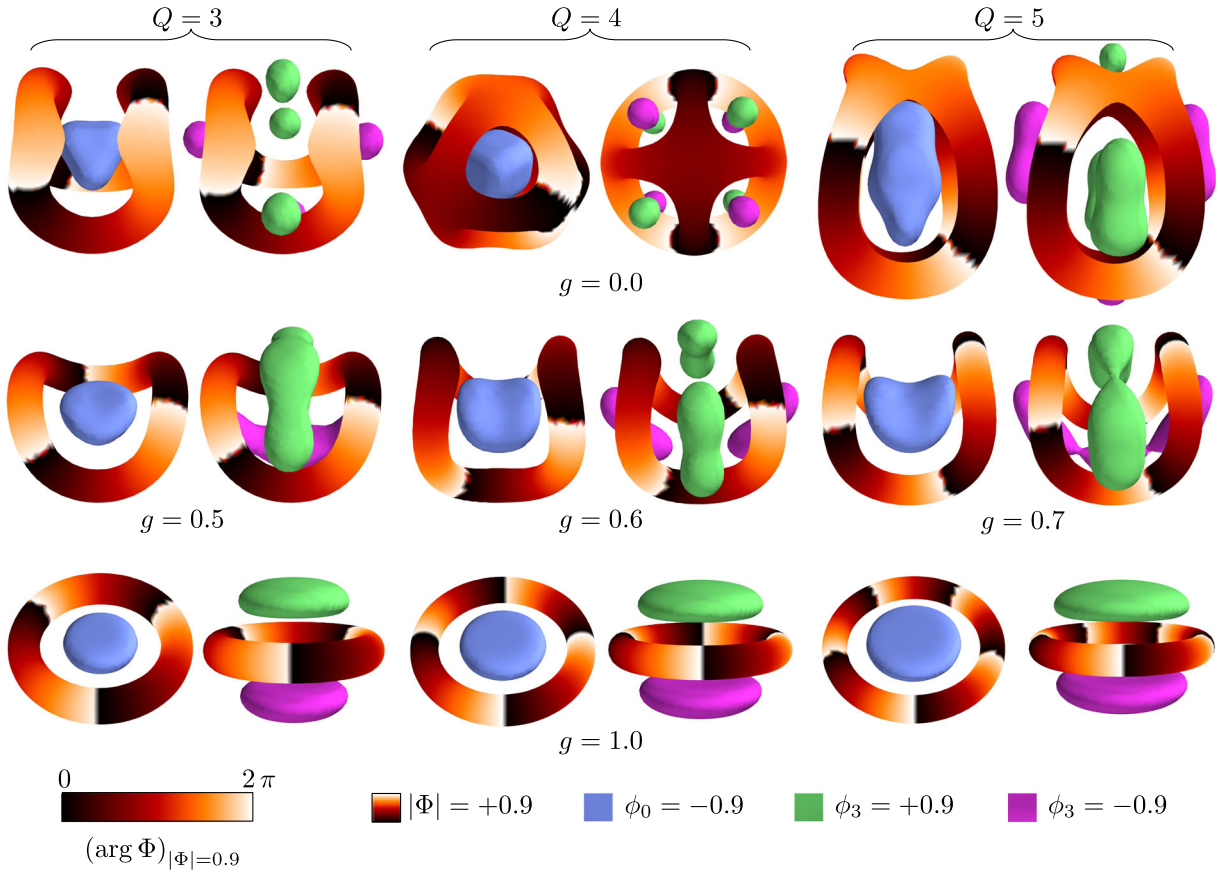

FIG. 10. Isosurfaces of the field components $\phi_0 = -0.9, \phi_3 = \pm 0.9$, and $|\Phi| = 0.9$, where $\Phi \equiv \phi_1 + i\phi_2$, of the $Q = 3, 4, 5$ gauged skyrmions for some values of g. The orientation in isospace is visualized using the field coloring scheme for the argument $\arg(\Phi) \in [0, 2\pi)$.

However, the solutions of the gauged Skyrme model in the strong coupling limit are different from the conventional axially symmetric hopfion classified by the Hopf invariant [72,73]. The field components of the toroidal gauged skyrmions displayed in Fig. 10 do not form linked or knotted loops.

VI. CONCLUSIONS

The objective of this work is to extend further previous analysis of the solution of the $U(1)$ gauged Skyrme model [41,42,59] by considering the solutions with topological charges up to $Q = 5$ coupled to the magnetic field. The gauged skyrmions are topologically stable and they carry a local magnetic flux that induces magnetic moment of the configuration.

We show that the backreaction of the magnetic field strongly affects the usual structure of multisoliton solutions, in particular, the discrete symmetry of ungauged skyrmions becomes broken due to the presence of a circular magnetic flux. The transformation to the toroidal skyrmions is observed in the strong coupling regime for all configurations we studied. A similar pattern was also observed for conventional skyrmions in the model with symmetry breaking potential [69].

The work here should be taken further by considering the electrically charged configurations with topological charge $Q > 1$; the pattern of evolution of corresponding $Q = 1$ gauged skyrmion was discussed in our previous work [59]. It might be also interesting to consider gauged skyrmions in a model with a symmetry breaking potential. We hope we can address these issues in our future work.

ACKNOWLEDGMENTS

We are grateful to E. Radu and D. H. Tchrakian for inspiring and valuable discussions. The numerical calculations were performed on the HybriLIT cluster at the JINR, Dubna.

[1] T. H. R. Skyrme, Proc. R. Soc. **260**, 127 (1961); Nucl. Phys. **31**, 556 (1962).
[2] T. H. R. Skyrme, Nucl. Phys. **31**, 556 (1962).
[3] N. S. Manton and P. Sutcliffe, *Topological Solitons* (Cambridge University Press, Cambridge, England, 2004).
[4] N. S. Manton, *Skyrmions—A Theory of Nuclei* (World Scientific, Singapore, 2022).
[5] G. E. Brown and M. Rho, *The Multifaceted Skyrmion* (World Scientific, Singapore, 2010).
[6] Y. M. Shnir, *Topological and Non-Topological Solitons in Scalar Field Theories* (Cambridge University Press, Cambridge, England, 2018).
[7] E. Witten, Nucl. Phys. **B223**, 422 (1983).
[8] E. Witten, Nucl. Phys. **B223**, 433 (1983).
[9] I. Zahed and G. E. Brown, Phys. Rep. **142**, 1 (1986).
[10] R. Battye and P. Sutcliffe, Phys. Rev. C **73**, 055205 (2006).
[11] R. Battye, N. S. Manton, and P. Sutcliffe, Proc. R. Soc. A **463**, 261 (2007).
[12] S. B. Gudnason and M. Nitta, Phys. Rev. D **94**, 025008 (2016).
[13] S. B. Gudnason and M. Nitta, Phys. Rev. D **91**, 085040 (2015).
[14] É. Dupuis, M. Haberichter, R. MacKenzie, M. B. Paranjape, and U. A. Yajnik, Phys. Rev. D **99**, 016016 (2019).
[15] L. R. Livramento and Y. Shnir, Phys. Rev. D **105**, 125019 (2022).
[16] S. B. Gudnason, Phys. Rev. D **93**, 065048 (2016).
[17] S. B. Gudnason and M. Nitta, Phys. Rev. D **94**, 065018 (2016).
[18] A. Jackson, A. D. Jackson, A. S. Goldhaber, G. E. Brown, and L. C. Castillejo, Phys. Lett. **154B**, 101 (1985).
[19] G. S. Adkins and C. R. Nappi, Phys. Lett. **137B**, 251 (1984).
[20] B. Schwesinger and H. Weigel, Nucl. Phys. **A465**, 733 (1987).
[21] H. Yabu, B. Schwesinger, and G. Holzwarth, Phys. Lett. B **224**, 25 (1989).
[22] H. Forkel, A. D. Jackson, and C. Weiss, Nucl. Phys. **A526**, 453 (1991).
[23] S. B. Gudnason and J. M. Speight, J. High Energy Phys. 07 (2020) 184.
[24] C. Naya and P. Sutcliffe, J. High Energy Phys. 05 (2018) 174.
[25] C. Naya and P. Sutcliffe, Phys. Rev. Lett. **121**, 232002 (2018).
[26] P. Sutcliffe, J. High Energy Phys. 08 (2010) 019.
[27] P. Sutcliffe, Mod. Phys. Lett. B **29**, 1540051 (2015).
[28] P. Sutcliffe, J. High Energy Phys. 04 (2011) 045.
[29] T. Sakai and S. Sugimoto, Prog. Theor. Phys. **113**, 843 (2005).
[30] M. F. Atiyah and N. S. Manton, Phys. Lett. B **222**, 438 (1989).
[31] L. Marleau, Phys. Rev. D **45**, 1776 (1992).
[32] L. Marleau, Phys. Rev. D **43**, 885 (1991).
[33] I. Floratos and B. Piette, Phys. Rev. D **64**, 045009 (2001).
[34] C. Adam, J. Sanchez-Guillen, and A. Wereszczynski, Phys. Lett. B **691**, 105 (2010).
[35] C. Adam, C. Naya, J. Sanchez-Guillen, and A. Wereszczynski, Phys. Rev. Lett. **111**, 232501 (2013).
[36] C. Adam and A. Wereszczynski, Phys. Rev. D **89**, 065010 (2014).
[37] S. B. Gudnason and M. Nitta, J. High Energy Phys. 09 (2017) 028.
[38] L. A. Ferreira and Y. Shnir, Phys. Lett. B **772**, 621 (2017).
[39] L. A. Ferreira, J. High Energy Phys. 07 (2017) 039.
[40] L. A. Ferreira and L. R. Livramento, J. Phys. G **49**, 115102 (2022).
[41] B. M. A. G. Piette and D. H. Tchrakian, Phys. Rev. D **62**, 025020 (2000).
[42] E. Radu and D. H. Tchrakian, Phys. Lett. B **632**, 109 (2006).
[43] B. J. Schroers, Phys. Lett. B **356**, 291 (1995).
[44] D. H. Tchrakian and K. Arthur, Phys. Lett. B **352**, 327 (1995).
[45] B. J. Schroers, Nucl. Phys. **B475**, 440 (1996).
[46] J. Gladikowski, B. M. A. G. Piette, and B. J. Schroers, Phys. Rev. D **53**, 844 (1996).
[47] Y. M. Shnir, Phys. Part. Nucl. Lett. **12**, 469 (2015).
[48] A. Samoilenka and Y. Shnir, Phys. Rev. D **93**, 065018 (2016).
[49] C. Adam, C. Naya, J. Sanchez-Guillen, and A. Wereszczynski, Phys. Rev. D **86**, 045010 (2012).
[50] C. Adam and A. Wereszczynski, Phys. Rev. D **95**, 116006 (2017).
[51] A. Samoilenka and Y. Shnir, Phys. Rev. D **95**, 045002 (2017).
[52] F. Navarro-Lérida and D. H. Tchrakian, Phys. Rev. D **99**, 045007 (2019).
[53] F. Navarro-Lérida, E. Radu, and D. H. Tchrakian, Phys. Lett. B **791**, 287 (2019).
[54] Y. Shnir and G. Zhilin, Phys. Rev. D **89**, 105010 (2014).
[55] A. Samoilenka and Y. Shnir, Phys. Rev. D **97**, 125014 (2018).
[56] V. A. Rubakov, JETP Lett. **33**, 644 (1981).
[57] C. G. Callan, Jr., Phys. Rev. D **25**, 2141 (1982).
[58] J. Cork, D. Harland, and T. Winyard, J. Phys. A **55**, 015204 (2022).
[59] L. R. Livramento, E. Radu, and Y. Shnir, SIGMA **19**, 042 (2023).
[60] C. G. Callan, Jr. and E. Witten, Nucl. Phys. **B239**, 161 (1984).
[61] R. A. Battye, S. Krusch, and P. M. Sutcliffe, Phys. Lett. B **626**, 120 (2005).
[62] R. A. Battye, M. Haberichter, and S. Krusch, Phys. Rev. D **90**, 125035 (2014).
[63] G. H. Derrick, J. Math. Phys. (N.Y.) **5**, 1252 (1964).
[64] M. Laue, Ann. Phys. (Berlin) **340**, 524 (1911).
[65] I. Bialynicki-Birula, Phys. Lett. A **182**, 346 (1993).
[66] S. Krusch and P. Sutcliffe, J. Phys. A **37**, 9037 (2004).
[67] T. Ioannidou, B. Kleihaus, and J. Kunz, Phys. Lett. B **643**, 213 (2006).
[68] Y. Shnir and D. H. Tchrakian, J. Phys. A **43**, 025401 (2010).
[69] S. B. Gudnason and M. Nitta, Phys. Rev. D **91**, 045027 (2015).
[70] L. D. Faddeev, *Quantization of Solitons* (Princeton, 1975), Preprint-75-0570, IAS.
[71] L. D. Faddeev and A. J. Niemi, Nature (London) **387**, 58 (1997).
[72] J. Gladikowski and M. Hellmund, Phys. Rev. D **56**, 5194 (1997).
[73] M. Kobayashi and M. Nitta, Phys. Lett. B **728**, 314 (2014).